THE ASTROPHYSICAL JOURNAL, 344:791–798, 1989 September 15

THE INFRARED EMISSION BANDS. II. A SPATIAL AND SPECTRAL STUDY OF THE ORION BAR

J. D. BREGMAN,[1] L. J. ALLAMANDOLA,[1] A. G. G. M. TIELENS,[1,2] T. R. GEBALLE,[3] AND F. C. WITTEBORN[1]
Received 1988 May 6; accepted 1989 March 2

ABSTRACT

We have studied the spectral and spatial distribution across the Orion Bar of the 3–14 μm emission, including hydrogen Brackett α and 12.8 μm [Ne II] emission lines and several "dust" emission features. The data indicate that the "dust" consists of three components; (1) "classical" dust with a temperature of $\sim$60 K accounting for emission longward of 20 μm, (2) amorphous carbon particles or polycyclic aromatic hydrocarbon (PAH) clusters ($\approx$400 C atoms) which produce broad emission features in the 6–9 and 11–13 μm bands, and (3) free PAHs which emit in sharper bands (most strongly at 3.3, 6.2, 7.7, 8.6, and 11.3 μm). The 3.3 and 11.3 μm features, which are due to C-H modes, are well correlated spatially, while the 7.7 μm band, due to C=C modes, has a different distribution than the 3.3 and 11.3 μm bands. We conclude that the sharp emission bands arise in the photodissociation transition region between the H II region and the molecular cloud and are not present in the H II region. The broad continuum feature extending from 11–13 μm is strong in both regions. Previous broad-band observations of the 10 and 20 μm flux distributions, which show that the 10 μm radiation extends farther into the neutral gas to the south than the 20 μm radiation, suggest that some of the 10 μm flux is supplied via a nonthermal mechanism, such as fluorescence.

Subject headings: infrared: sources — infrared: spectra — interstellar: grains — interstellar: molecules — nebulae: H II regions — nebulae: Orion Nebula

I. INTRODUCTION

A number of infrared emission features, collectively known as the unidentified infrared (UIR) bands, have been observed in a variety of astronomical objects, including planetary nebulae, H II regions, reflection nebulae, and galactic nuclei, all objects in which UV radiation sources illuminate dusty regions. The identification of these features has proven a difficult task. Their most likely origin is from the CH and CC stretching and bending modes of carbonaceous compounds. Three types of carbonaceous material have been proposed as the carrier of the UIR bands, hydrogenated amorphous carbon (soot or HAC) particles (Duley and Williams 1981), quenched carbonaceous composite (QCC) particles (Sakata *et al.* 1984), and polycyclic aromatic hydrocarbon (PAH) molecules, the building blocks of soot particles (Leger and Puget 1984; Allamandola, Tielens, and Barker 1985). All three materials are intimately related. Both HAC and QCC particles are forms of amorphous carbon which Robertson and O'Reilly (1987) have shown are composed of clusters of PAH molecules. Thus, it is likely that amorphous carbon particles and free PAH molecules coexist in objects showing the UIR bands.

Several analyses of the infrared emission features strongly suggests that molecular PAHs with $\sim$20 carbon atoms are largely responsible (e.g., Sellgren 1984; Cohen *et al.* 1986; deMuizon *et al.* 1986). These PAHs have been calculated to have an abundance relative to hydrogen of $\sim 2 \times 10^{-7}$, which corresponds to 1% of the elemental carbon, making these complex molecules only slightly less abundant than CO. Although the infrared spectra of single, simple, small PAHs do not provide a good fit to the observed interstellar spectra, the good comparison with soot spectra suggests that a collection of PAHs could provide a reasonable fit (Allamandola, Tielens, and Barker 1985).

The Orion Bar is an ionization front which is viewed nearly edge-on, making it an ideal object in which to study the distribution of the UIR features across an H I–H II interface (Becklin *et al.* 1976). The H II region north of the Bar provides a much stronger UV field than exists south of the Bar. Becklin *et al.* (1976) showed that there is 10 μm emission associated with the ionization front, either at the interface of the ionized and neutral gas, or just outside the ionized region. Aitken *et al.* (1979) obtained spectra of the Bar from 8–13 μm, showed that it had the strong unidentified features at 8.6 and 11.3 μm, and concluded that the features were strongest just outside the ionized region.

Sellgren (1981) mapped a large part of the Orion nebula with a 30″ beam, both in the unidentified emission feature at 3.3 μm and in the continuum at 3.5 μm. She concluded that the feature was strongest at the interface of the ionized and neutral gas, with the emission across the H II region attributable to material in the background interface of the H I and H II regions. The greater intensity of the emission feature at the Bar would therefore be due to limb brightening.

Important clues to the carriers of the UIR bands and the continuum may lie in the detailed variations of their relative strengths across an H I/H II interface. Previously published studies of these bands near the Orion Bar have neither included enough of the bands nor used high enough spatial resolution to provide the needed detail. Therefore, we have used the NASA-Ames mid-IR grating spectrometer, which covers the entire 8–13 μm window simultaneously, to measure the spatial distributions of the 7.7, 8.6, and 11.3 μm UIR bands, the Ne II 12.8 μm emission line, and the underlying continuum in this region. In addition, we obtained separate measurements of the 3.3 μm UIR feature and the Brackett alpha emission line of ionized hydrogen in a similar sized beam using the grating spectrometer at UKIRT. We also obtained spectra in the 5.2–8

[1] Space Sciences Division, NASA Ames Research Center.
[2] Space Sciences Laboratory, University of California, Berkeley.
[3] Joint Astronomy Center, Hilo, Hawaii.

μm region in a larger beam from the Kuiper Airborne Observatory (KAO), which allows us to correlate the 6.2 μm and 7.7 μm features with the features at other wavelengths.

In this paper, observations of the IR emission features are compared to the hypothesis that PAH molecules are the carriers of the UIR bands. Some of the arguments in support of the molecular-sized PAH hypothesis are nonunique, and both HAC or QCC particles could work as well. However, we will argue that the IR emission arises from three components, PAH molecules, amorphous carbon particles, and larger dust grains. Each component accounts for a particular aspect of the IR spectrum, and a single component is unlikely to account for the entire spectrum.

II. OBSERVATIONS

The Orion Bar was observed from the KAO in 1983 November with a 24 detector, liquid helium cooled, grating spectrometer (Witteborn and Bregman 1984). The spectrometer covered the entire 5.2–8.0 μm range simultaneously with a spectral coverage of 0.12 μm per detector. We used a 2′ chop and 21″ aperture. Observations were obtained with the same instrument from 7.8 to 12.8 μm, with a spectral coverage of 0.22 μm per detector, at the NASA/Steward 60″ (1.5 m) telescope on Mount Lemmon, Arizona, in 1984 January and from 8.2 to 13.2 μm in 1985 February. In 1984 January we used a 6″ aperture and a 2′ N-S chop, while in 1985 February we used a 6″ aperture, and a 2′ E-W chop in order to avoid chopping onto spatially variable emission present in the H II region to the north. Observations of the 3.3 μm feature and Brackett alpha were obtained in 1984 December from the UKIRT using the seven channel InSb grating spectrometer with a 5″ aperture and 2′ chop, both N-S and E-W. There is some difference in the spectra obtained with different chop directions due to the reference position for the N-S chop being located on a ridge of

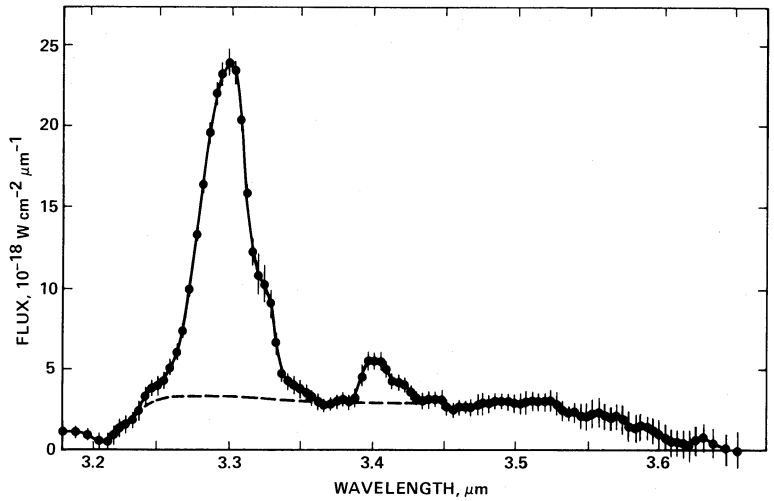

FIG. 1*a*

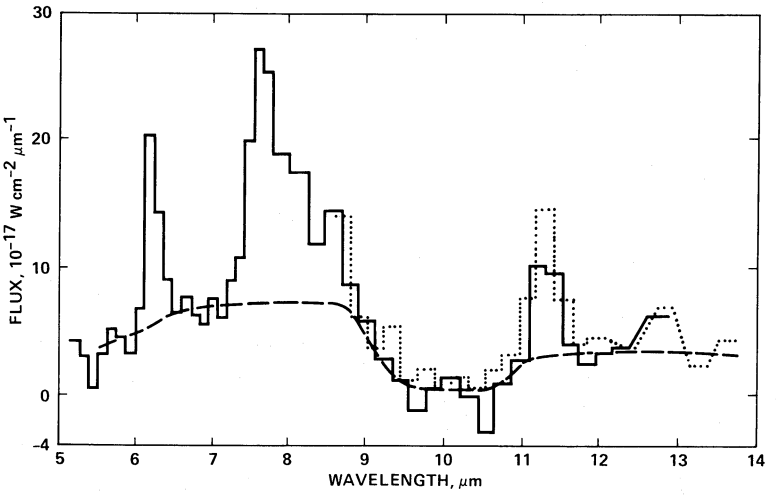

FIG. 1*b*

FIG. 1.—(*a*) The 3.17–3.70 μm spectrum of the Orion Bar at position 4 in a 5″ aperture. The dashed line indicates the broad pedestal upon which the sharp 3.29 and 3.40 μm emission bands are superimposed. (*b*) The 5–13 μm spectrum of the Orion Bar. The solid line is data obtained in a 21″ aperture centered on position 4 from the Kuiper Airborne Observatory (5–8 μm), and in 6″ apertures from the NASA Mount Lemmon 1.5 m telescope (8–12.8 μm). The Mount Lemmon data consists of four positions centered on position 4 which were coadded and then normalized to the KAO data in the region of overlap. The dotted line is data obtained in a 3″ aperture at several positions from the IRTF, coadded, and then normalized to the Mount Lemmon data. The dashed line roughly indicates the broad underlying pedestals from $\approx$6–9.5 μm and 10.5 > 13.5 μm. All data were obtained with a north-south chop.

emission at the boundary of the dark bay and the H II region to the north. Therefore, just the data taken with the E-W chop direction was used for studying the spatial distribution of the UIR features. In all cases, standard stars were used to cancel the atmospheric and instrumental effects, and to provide absolute flux calibration. The standards were β And on the KAO, α Tau at Mount Lemmon, and ξ Ori and Sirius at the UKIRT. Standard beam-switching techniques were employed. All positions are referenced to position 4 (Becklin *et al.* 1976), which we took as 11″ south and 45″ west of θ^2 Ori A. We estimate a relative accuracy of $\pm 1''$ between the different positions, and an absolute accuracy of $\pm 2''$.

Figure 1*a* shows the 3.1–3.7 μm spectrum of position 4. Figure 1*b* is a composite spectrum from 5.2 to 13.6 μm at the same location. In Figure 1*b*, data from Mount Lemmon were scaled to the data taken from the KAO by normalizing the overlapping channels. The dotted line depicts data obtained with the same spectrometer operating from 8.6–13.6 μm on the IRTF in 1982 November. The standard star in that case was β Ori, and the chopper throw was 20″ N-S.

The intensities of the UIR features were measured by subtracting the integrated strengths of the features from the adjacent continua except in the case of the 7.7 μm band in the spectra obtained at Mount Lemmon. Since only the shoulder of the 7.7 μm band is observable from the ground, and the continuum is nearly zero longward of the feature, we used the flux at 8.2 μm as an indicator of the strength of the 7.7 μm band. Justification of this method is given below.

III. DESCRIPTION OF DATA

a) Spectra

In Figure 1*a* the 3.29 μm and the 3.40 μm narrow features are plainly evident, as well as the broad underlying component indicated by the dashed line, extending from $\sim$3.2 to 3.6 μm. The 5.2–13.6 μm spectrum in Figure 1*b* contains the narrow UIR features and an underlying "continuum" (indicated by the dashed line), which appears to be composed of two broad features. The extent of each of the broad features is difficult to define, but is $\sim$6.0–9.5 μm and 10.5–14 μm.

Figure 2 shows a sequence of spectra obtained from the KAO starting 10″ north of position 4 (*top spectrum*) and moving in 10″ steps south across the bar. A north-south chop was used. The emission is equally strong at position 4 and 10″ south of position 4, with a dropoff both to the north and south. There is an apparent shift of the center of the 6.2 μm feature to longer wavelengths going to the south. We also observe this effect in the 11.3 μm feature using a N-S chop, but not when using an E-W chop. Therefore, this effect is probably due to emission from the H II region in the reference beam.

b) Spatial Distributions

The spatial distributions of the features and the Ne II and Brα lines are shown in Figure 3. The zero position of the plot is position 4 as defined by Becklin *et al.* (1976). Offsets from zero are in seconds of arc north or south. The intensity of the Brα line is strong in the H II region to the north, decreases rapidly in strength at the edge of the bar and then declines slowly to the south. The residual intensity to the south is due to ionized gas in front of the neutral gas in the bar.

Due to the poor transmission of the Earth's atmosphere shortward of 8 μm, the shortest wavelength data point at 8.2 μm must be used to determine the spatial distribution of the 7.7 μm feature. (The spatial resolution of 21″ from the KAO was too low to allow a direct comparison to the Mt. Lemmon data in Figure 3.) Since the broad 6–9.5 μm continuum feature might contribute to the narrow component at 8.2 μm, we compared the 8.2 μm data to data between 8.8 and 9.2 μm which is on the wing of the broad feature. The results are shown in Figure 4 and demonstrate that the spatial distributions are quite different at the two wavelengths. The broad distribution of the 9.2 μm emission is similar to the distribution of the flux at 11.8 μm (see Fig. 5), while the spatial distribution of the 8.2 μm emission is similar to that of the UIR features.

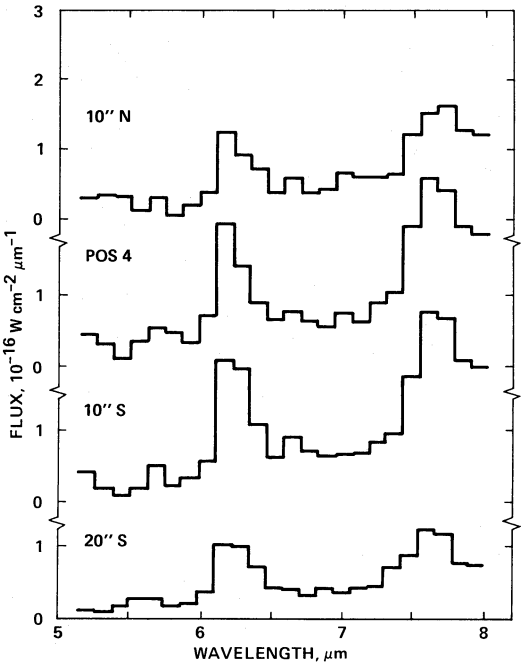

FIG. 2.—Spectra of the Orion Bar at various positions relative to position 4. The top spectrum corresponds to 10″ north of position 4, the second at position 4, the third 10″ south of position 4, and the bottom spectrum 20″ south of position 4.

IV. DISCUSSION

a) Spatial Distribution of the Emission

It is clear from Figure 3 that the spatial distributions of the 3.3, 7.7, and 11.3 μm features are quite similar, with the 7.7 μm feature peaking more sharply than the others. The Ne II line peaks 5″ north of the UIR features and, as the Brα intensity continues to increase to the north, must correspond to a peak in the column density of this ion. The spatial distributions of the UIR features are consistent with emission from a narrow region extending into the neutral gas adjacent to the H II region. While the 8.6 μm feature peaks 5″ south of the other features, deeper into the neutral gas, the data obtained with a N-S chop direction do not confirm this behavior. Since the 8.6 μm band is weak and superposed on the shoulder of the broad 8 μm feature and the narrow 7.7 μm band, the differences may not be significant.

The behavior of the 11.3 μm feature is quite different in the two data sets corresponding to the N-S and E-W chop. The 11.3 μm feature was in two channels each time. The ratio of the short wavelength to long wavelength channel is shown in Figure 6 for the two dates. In the data using the N-S chop, there is a systematic shift of the feature to longer wavelengths

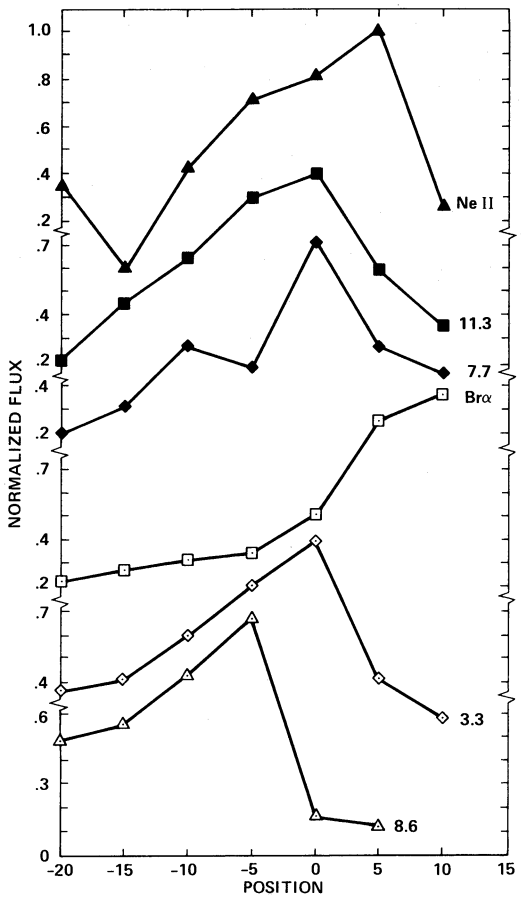

FIG. 3.—The spatial distribution of four of the sharp emission bands and two emission lines is shown as a function of position across the Orion Bar. The position axis is in units of arcseconds relative to position 4 with positive values indicating north. The curves are (from top to bottom): Ne II (*filled triangles*); 11.3 (*filled squares*); 7.7 (*filled diamonds*); Brα (*open squares*); 3.3 (*open diamonds*); and 8.6 (*open triangles*).

going from north to south, while in the data taken with an E-W chop, this trend is absent. Figure 5 shows that the intensity of the feature was nearly the same for both E-W and N-S chops at the three southern-most positions, but the feature observed in the northern position using a N-S chop was progressively weaker than when observed with an E-W chop. This behavior implies the existence of a ridge of emission to the north in which emission occurs in the 11.3 μm feature at slightly longer wavelengths than in the Bar. Indeed, the map of the 3.3 μm feature (Sellgren 1981) shows a ridge of emission 2′ to the north where the H II region meets the dark bay, a region of foreground obscuration. If the 11.3 μm band is from PAH molecules, then the observed shift to longer wavelengths of the feature in the ridge could be contributed to by emission from a molecule which has a feature slightly longward of 11.3 μm, or from emission from vibrational levels above $v = 1$, which are shifted in wavelength relative to the $v = 1$–0 transition (Barker, Allamandola, and Tielens 1987). Figure 2 shows similar behavior for the 6.2 μm feature.

The closer similarity between the distribution of the 3.3 and 11.3 μm features than between either of them and the 7.7 μm feature is consistent with polycyclic aromatic hydrocarbons being the material responsible for the features. In the PAH model, the 7.7 μm feature is due to the C=C skeletal modes of the molecules, while the 3.3 and 11.3 μm features are due to C-H stretching and bending modes, respectively (Allamandola *et al.* 1985). Figure 7 shows that the 6.2 μm feature, which is also due to a C=C mode, correlates very well with the 7.7 μm feature. If there is a mixture of molecules of different sizes or varying fractions of hydrogenation (i.e., different ratios of C=C to C-H bonds), then the 7.7 μm feature need not correlate as tightly with the 3.3 and 11.3 μm features as with the 6.2 μm feature. Similarly, the 3.3 and 11.3 μm features should also correlate with each other more tightly than with the 6.2 or 7.7 μm features, although energetics will strongly influence the 3.3 and 11.3 μm feature intensities. That this is observed provides support for the PAH hypothesis. The indication of anharmonicity effects on the profiles of the sharper features such as the 11.3 and 6.2 μm bands, points to emission from highly vibrationally excited free molecules rather than particles. The effects

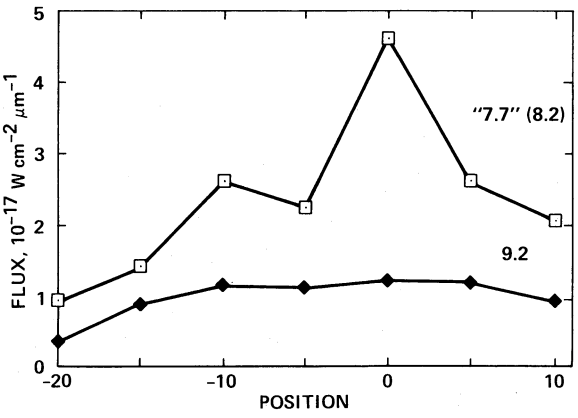

FIG. 4

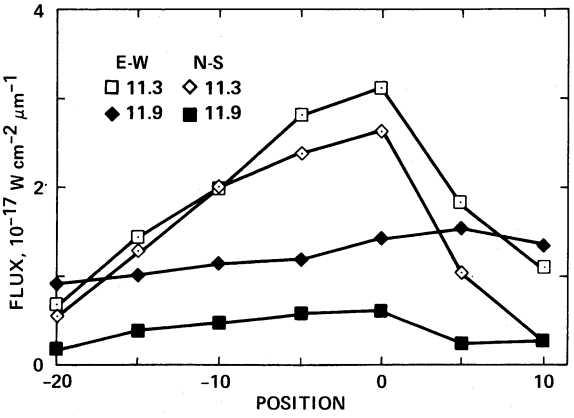

FIG. 5

FIG. 4.—The distribution of the flux at 8.2 μm (the wing of the 7.7 μm emission band; *open squares*) and 9.0 μm (the pedestal; *filled diamonds*) are shown as a function of position relative to position 4 as described for Fig. 3.

FIG. 5.—The distribution of the fluxes in the sharp 11.3 μm emission feature (*open symbols*) and the broad underlying pedestal (represented by the sum of the flux in four adjacent channels centered at 11.8 μm, *filled symbols*) are shown for the N-S and E-W chop directions as a function of position relative to position 4.

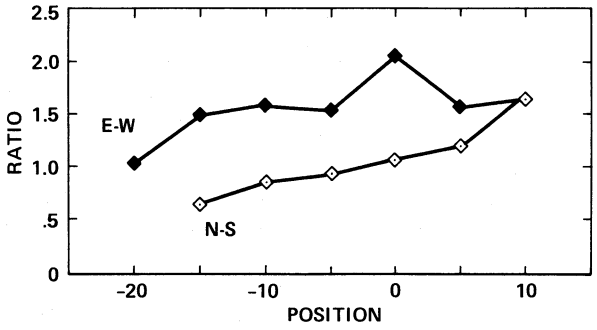

FIG. 6

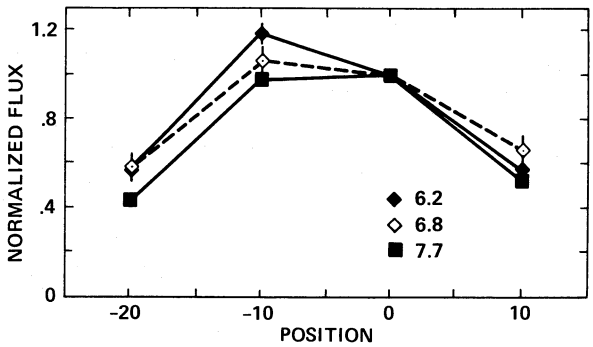

FIG. 7

FIG. 6.—The distribution of the ratio of the short- to long-wavelength channels at the position of the 11.3 μm emission band are shown for a north-south (*open diamonds*) and east-west (*solid diamonds*) chop. Positions are as described for Fig. 3.

FIG. 7.—The distribution of the 6.2 μm (*solid diamonds*) and 7.7 μm (*solid squares*) emission bands and emission at 6.8 μm (*open diamonds*) (measured from the KAO) as a function of position relative to position 4. The curves have been normalized to 1 at position 4.

of anharmonicity are particularly dramatic in the 3 μm region where they may be responsible for the weak 3.4 μm feature superposed on the broad plateau (Barker *et al.* 1987). In regions of high excitation, this emission from higher levels is important and these aspects of the spectrum will be prominent. Such behavior has recently been observed for locations south of position 4, where the 3.4 μm feature and some of the other components discovered by deMuizon *et al.* (1986) in the 3–4 μm region, become progressively stronger relative to the 3.29 μm emission, and where smaller molecules, whose CH bonds are more likely to be excited to higher vibrational levels, can survive (Geballe *et al.* 1989).

b) *Modeling the Spatial Distribution*

The Orion nebula is an excellent example of an H II blister on the edge of a molecular cloud (see, e.g., Fig. 8, adapted from Zuckerman, 1973). The ionized gas is streaming away from the H II/H I interface (molecular cloud) into a low-density surrounding medium. The Orion bar represents such an H II/H I interface seen almost edge on, as evidenced by, for example, the O I λ8446 line emission (Münch and Taylor 1974). Within the concept of an H II blister model, the observed distribution of the UIR features and the Brα and Ne II emission lines can be interpreted in terms of changes in the viewing geometry of the emitting gas. In our analysis, we will assume that the gas density does not vary along our N-S scan. The observed intensity variations are then solely due to variation in the path length through the emitting gas (i.e., geometry). With this assumption, the shape of the ionization front along our N-S scan is traced by the spatial distribution of the Brα line (see, e.g., Fig. 3). The IR emission can then be modeled geometrically by drawing curves parallel to this derived shape of the H II/H I interface at different aspect ratios (i.e., depth to beam-width ratios).

The curves in Figure 9 show the distribution which would be observed in a 5″ beam for varying thicknesses of uniform emission. The 0″ curve (*open squares*) is emission calculated by integrating along each line of sight and assuming it arises from a species which is present just along the interface of the H II region. The other curves show the expected emission from thicker and thicker zones of emission from the neutral region.

We now compare the curves with the actual data in Figure 3. The Ne II line shows the characteristics of the 0″ curve, consistent with Ne II emission from a thin layer near the boundary of the H II region and the neutral gas. The optical depth to ionizing photons in the neutral gas is very high, so one does not expect neon to be ionized very deeply into the neutral gas, while the neon in the H II region is mainly in the form of Ne III. The 3.3 and 11.3 μm features are well matched by emission from a zone 15″ thick, while the 7.7 μm feature seems more consistent with emission from a 5″ thick zone. The 8.6 μm feature cannot be fitted with this model even if one assumes that it arises from a zone inside the neutral gas.

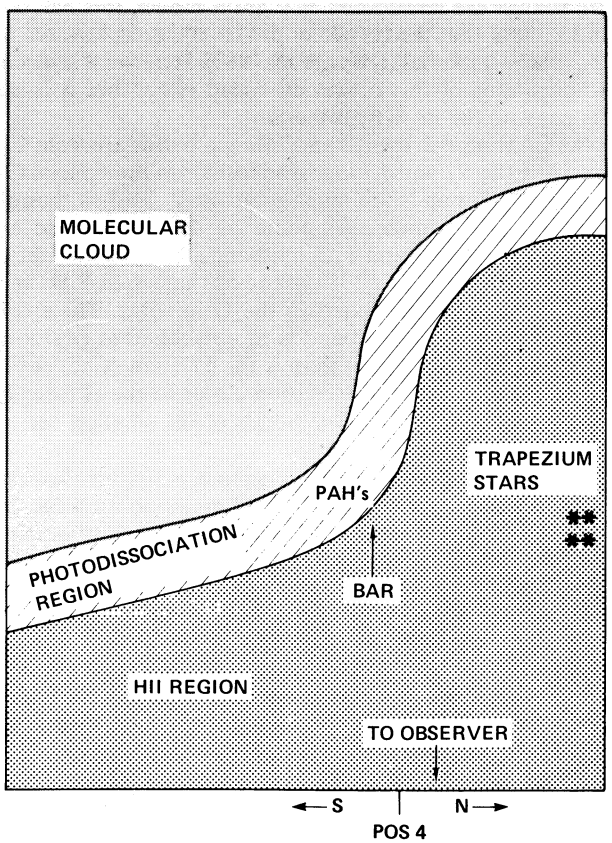

FIG. 8.—Schematic representation of the model used to calculate the distribution of bands and emission lines shown in Fig. 3. The view is from above the Orion nebula region with the observer in the plane of the paper and toward the bottom of the page. South is to the left, and north to the right. The distance from the Trapezium stars to the Bar (at position 4) is ~2′ (8×10^{17} cm).

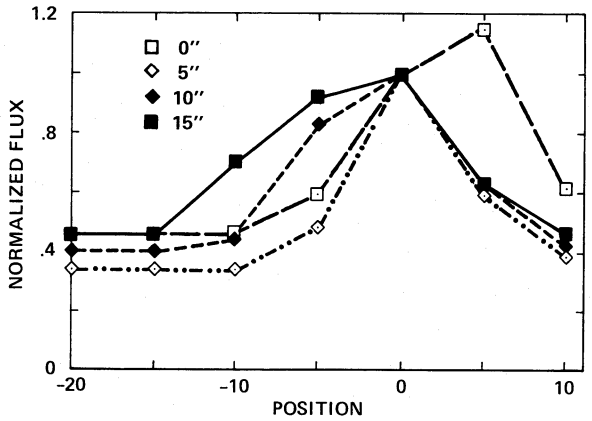

FIG. 9.—The distribution of flux as a function of position relative to position 4 in a 5″ aperture using the model described in the text. All the curves are normalized to 1 at position 4. The different symbols represent emission from regions (labeled Photodissociation Region in Fig. 8) of different thicknesses: *Open squares*, 0″; *open diamonds*, 5″; *filled diamonds*, 10″; and *filled squares*, 15″ thickness.

c) *Destruction of PAHs in the* H II *Region*

These results have some interesting implications for the excitation and survival of the material responsible for the UIR features. The observations show that the dominant emission in the features arises from the neutral gas, in agreement with the spatial mapping done by Sellgren (1981) and Aitken *et al.* (1979). Within the framework of a grain model, this has been taken to imply that the carrier of the IR emission features is a rather volatile material (Dwek *et al.* 1980). Here we will discuss the implications of this observation and show that it is also consistent with the PAH hypothesis.

In the PAH model, the 3.3 and 11.3 μm bands are from C-H bonds while the 6.2 and 7.7 μm bands are from the skeletal C-C bonds. The C-H bonds are much more easily broken than the C-C bonds, so the molecules could be dehydrogenated and thus not show the 3.3 and 11.3 μm bands, but still emit at 6.2 and 7.7 μm. Tielens *et al.* (1987), showed that small PAH molecules will be dehydrogenated in the Orion Bar. The spatial distribution of the 7.7 μm band is more peaked at position 4 (close the H I/H II interface) than is the 11.3 μm band, consistent with increased dehydrogenation closer to the H II region. Inside the H II region, the C-C bonds of the smallest carriers may be ruptured as well.

Since the density inside the H II region is ~ 10 times less than in the Bar, there is possibly some UIR emission from the H II region. The relative amounts of emission can be estimated as follows. If the PAHs are as abundant relative to hydrogen in the H II region as in the neutral gas, then the relative contribution from each region is approximately given by the relative hydrogen column densities through these regions. For the ionized gas, this corresponds to a total hydrogen column density of $\sim 2.6 \times 10^{21}$ cm^{-2} (using an emission measure of 5.2×10^{6} cm^{-6} pc and a density of 6×10^{3} cm^{-3}; Martin and Gull 1976). The corresponding hydrogen column density in the neutral zone is given by

$$N_{\rm H} \approx N_{\rm H}/A_v * A_v/\tau_{\rm uv} * \tau_{\rm uv} \approx 3.4 \times 10^{21} \text{ cm}^{-2} ,$$

where we have assumed that the features are excited by photons around 2000 Å (e.g., the $\Pi \rightarrow \Pi^*$ transition in PAHs), used standard dust parameters (Savage and Mathis 1979), and assumed that all the photon energy is absorbed within a uv optical depth of 3. PAHs can also be undergo higher energy $\sigma \rightarrow \sigma^*$, $\Pi \rightarrow \sigma^*$, and $\sigma \rightarrow \Pi^*$ transitions inside the H II region. These transitions give rise to a strong absorption band around 15 eV. Since the stellar uv energy density below 13.6 eV is about half the total available luminosity for a 40,000 K star (such as Θ^1C Ori), we would expect that if small PAHs were present inside the H II region, they would dominate the emission in the features and, thus, we conclude from the observations that they are not as abundant in the H II region as in the neutral gas.

This conclusion may seem somewhat surprising at first sight since the ionized material in a blister H II region originated in the neutral molecular cloud. It implies, therefore, that the smaller PAHs are destroyed in the ionized gas. Probably, this destruction is due to the absorption of individual very energetic uv photons ($h\nu \approx 20$ eV) or to two photon events, leading to fragmentation of an aromatic ring by bond rupture or Coulomb explosion (Leach 1987). For fragmentation of an aromatic ring, two three-electron bonds have to be broken simultaneously, which takes at least 11.5 eV (Benson 1965). In the (neutral) diffuse interstellar medium, where uv photons are less energetic than 13.6 eV, these processes have a very low probability even for a 20 carbon atom PAH (see, e.g., Crawford, Tielens, and Allamandola 1985). However, inside an H II region more energetic photons are available and the fluxes are higher. Here, the lifetime of a PAH will be much less. Destruction of small (≤ 100 Å) carbon grains by chemical reactions is important only at densities of 10^5 cm^{-3} or higher (Draine 1979) and consequently this process is unimportant for the Orion region.

A crude estimate for the probability of fragmentation can be made using unimolecular rate theory (see, Dalgarno 1975). Representing the molecule by a collection of oscillators of equal frequency, the lifetime of a 20 carbon atom PAH containing 20 eV of vibrational excitation energy is $\sim 3 \times 10^5$ s. Because the radiative lifetime is ~ 0.1, the probability of photofragmentation upon absorption of a 20 eV photon is $\sim 3 \times 10^{-7}$. With a uv absorption cross-section of 5×10^{-16} cm^2 and a photon flux of 10^{13} photons cm^{-2} s^{-1}, appropriate for the H II region close to the bar, we find a uv absorption time scale of $\sim 2 \times 10^2$ s and thus a photofragmentation time scale of ~ 20 yr. Larger emitters may be destroyed by multiple photon absorption events as suggested by Sellgren (1984). For example, a three-photon event would occur about every 10 yr, leading to 60 eV of internal excitation energy. In contrast, in the neutral zone a three-photon event would deposit only ~ 30 eV. Probably, 60 eV of internal excitation is sufficient to fragment much larger PAHs. Thus, while the lifetime of small PAHs in the diffuse interstellar medium is probably comparable to that of graphitic dust grains (Crawford, Tielens, and Allamandola 1985), in H II regions, PAHs will be destroyed on a time scale much shorter than the expansion timescale of the H II region ($\approx 10^5$ yr).

d) *Excitation of the PAHs*

Since the UIR features are present in the neutral gas, they must be able to be excited by photons less energetic than 13.6 eV. The data from Becklin *et al.* (1976) show that the broadband 10 μm emission extends farther to the south than the 20 μm emission. Since the inferred dust temperature is ~ 60 K, the 20 μm emission can probably be attributed to thermal emission from warm dust grains heated by UV photons, although PAH plane bending modes can contribute. The peak of the 20

μm emission is largely determined by the optical depth of the gas and dust to UV photons, resulting in a falloff of the dust temperature with increasing depth into the neutral gas. In contrast, the 10 μm emission is dominated by the UIR features. Since it extends deeper into the neutral gas than the 20 μm emission, the process that excites the UIR features cannot be thermal, but must be a nonthermal process, such as fluorescence.

e) *The "Continuum"*

In Figure 5 is plotted the spatial distribution of the narrow 11.3 μm UIR feature and the 11.8 μm "continuum," which we will use to characterize the broad feature extending from 9.5–14 μm. Both the N-S and E-W chop data are shown. The intensity of the broad feature in the N-S chop is less than half of the intensity observed with an E-W chop. However, the 11.3 μm feature is nearly the same in the two chop directions. There appears to be a ridge of emission in the 11.3 μm feature to the north which depresses the points north of 5″ south relative to the E-W chop direction (a ridge of emission is present on the 3.3 μm maps obtained by Sellgren 1981). Figure 5 shows that there are marked differences in spatial behavior at the two wavelengths, and that while the 11.3 μm feature is stronger to the south, the 11.8 μm emission (continuum) is stronger to the north, extending into the H II region. Thus, for the first time we see a clear difference in the distribution of a broad continuum feature and narrow UIR feature. Note that the distribution of the broad 6–9 μm feature as measured at 9 μm (Fig. 4) is flat, similar to the distribution of the 11.8 μm continuum, indicating a similar origin for these two broad features.

From an examination of the spatial behavior of the spectra of the Orion bar as well as of the spectral variations in other objects that show the emission features, we conclude that there are actually two components contributing to the 3–13 μm emission; PAH molecules which are responsible for the "narrow" emission features at 3.3, 6.2, 7.7, and 11.3 μm and amorphous carbon particles which produce the broad "continuum" emission features (see, e.g., § IV*a*; see also Allamandola, Tielens, and Barker 1987; Goebel 1987). As has been discussed in § IV*c*, small PAHs ($\approx$20 C atoms) cannot survive in the strong UV radiation field inside H II regions. Amorphous carbon particles, which are much larger, will not be destroyed inside H II regions by photofragmentation processes.

The differences in the destruction timescales of PAHs and amorphous carbon grains may also be able to explain the striking difference in the IR spectra of sources that show the emission features. For example, the IR spectrum of the planetary nebula NGC 7027 is dominated by the strong, broad continuum features with relatively weak narrow emission features on top of them (Russell, Soifer, and Willner 1977). In contrast, the Red Rectangle (HD 44179) shows little emission in the broad continuum features and the IR spectrum is actually dominated by the narrow emission features (Cohen *et al.* 1986). The spectrum of the Orion bar falls between these two extreme cases. It seems likely that the same processes are responsible for the relative ratios of the PAHs to the amorphous carbon grains in these regions. We note that NGC 7027 is powered by a central star with an effective temperature of $\sim$200,000 K (Russell *et al.* 1977), and therefore has copious amounts of high-energy UV photons as attested to by, for example, the presence of O V and N VI (Aller and Minkowski 1956). Thus, even larger PAHs can be destroyed in the high-excitation region of this nebula than in the Orion nebula ($T_{\rm eff}$ of Θ^1C Ori is $\sim$40,000 K) and large amorphous carbon grains can be sufficiently excited to emit in the mid-IR. In contrast, the Red Rectangle is a reflection nebula with an illuminating A0 star and very little ionized gas (Cohen *et al.* 1976). Thus, once out of the intense UV field of the inner portion of the nebula, even small PAHs with $\sim$20 carbon atoms can contribute to the emission from this nebula. Moreover, in the Red Rectangle, the spectrum of the illuminating star contains many photons around 2000 Å sufficiently energetic to excite the Π electron system of the PAHs. This will lead to emission in the bands but not destroy the molecules (Geballe *et al.* 1989).

There is a broad feature (the "plateau") underlying the 3.3 μm band as well (Geballe *et al.* 1985) which we examined to see if it had the same distribution as the 11.8 μm broad feature, or if it behaved similarly to the narrow features. As is apparent from Figure 10, the 3.3 μm narrow band and the broad component (measured at 3.35 μm) have similar peaked distributions, quite different from the broad distributions shown by the 11.8 and 9 μm continua. Since the plateau emission is also absent from the H II region, the material responsible for it cannot survive in that environment, and thus this plateau is likely to be molecular emission. Thus, like the features at 11.3 and 3.3 μm, we attribute the broad 3–3.6 μm feature to fluorescence by PAHs rather than emission by large dust grains. This is not too surprising as emission at 3 μm implies high excitation and, thus, molecular fluorescence, a conclusion that led originally to the suggestion of emission from molecular sized species. Recent observations show spatial variations in the structure in the 3.1–3.6 μm plateau which also point to a molecular origin for the plateau emission (Geballe *et al.* 1989).

The longer wavelength broad features could be due to thermal emission from warm carbon grains, but temperatures of $\sim$400 K are required to produce the 6–9 μm feature and 300 K for the 11–13 μm feature. Becklin *et al.* (1976) showed that even for very small graphitic grains the temperature was unlikely to be above 300 K at position 4. Since temperature is a very weak function of grain size, it is unlikely that the 6–9 μm broad feature can be due to dust grains at an equilibrium temperature of 400 K. Instead, we attribute the feature to non-

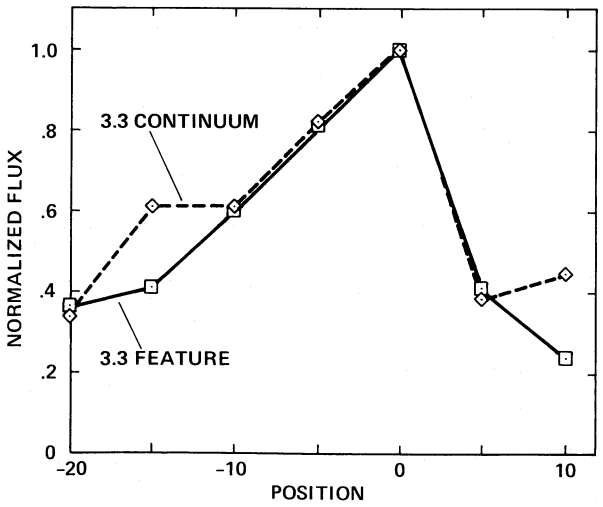

FIG. 10.—The distribution of the 3.28 μm sharp emission feature (*squares*) and the nearby plateau at 3.35 μm (*diamonds*, representative of the broad pedestal) as a function of position relative to position 4.

thermal emission from small dust grains or PAH clusters heated by single ultraviolet photons. Following Leger and d'Hendecourt (1987), we calculate that these dust grains contain ~400 carbon atoms, assuming 6 eV photons and the heat capacity appropriate for C-C bonds in PAH molecules.

V. SUMMARY

We have studied the 3–13 μm emission of the Orion Bar spectroscopically and spatially. We conclude that:

1. There are three emission components, one from "classical" dust that accounts for the bulk (not all) of the emission longward of 20 μm, a second one from large amorphous carbon grains or PAH clusters (containing on the order of 400 C atoms) accounting for the broad features (6–9 and 11–13 μm), and a third from PAH molecules (containing between 20 and 50 C atoms) that accounts for the sharp bands (e.g., 3.3, 6.2, 7.7, 8.6, and 11.3 μm plus other weaker features).

2. Although the spatial distribution of all the sharp features generally correlate, there are minor but revealing variations in their relative intensity distributions. The pair of features at 3.3 and 11.3 μm correlate with each other as do the pair at 6.2 and 7.7 μm. However, the 3.3 and 11.3 μm pair do not correlate tightly with the 6.2 and 7.7 μm pair. This is consistent with the 3.3 and 11.3 μm features arising from the C-H stretching and bending modes, respectively, of PAHs while the 6.2 and 7.7 μm features come from the C=C skeletal mode of PAHs.

3. Modeling of the emission shows that the 3.3 and 11.3 μm features arise in a 15″ thick zone just behind the ionization front, while most of the 7.7 μm feature comes from a 5″ thick zone just behind the ionization front. The features can thus be excited by photons less energetic than 13.6 eV. The different spatial distributions observed between the features assigned to C-H and C-C modes is consistent with increased dehydrogenation closer to the H II region.

4. The long-wavelength broad features (6–9 and 11–13 μm) that make up the "continuum" have a different distribution than the narrow features, and most likely arise by nonequilibrium emission from amorphous carbon grains or PAH clusters. In contrast, the 3–3.6 μm broad feature has the same distribution as the narrow UIR features, and therefore also originates from molecular PAHs. PAH molecules in the 20–50 C atom size range probably cannot survive the high-energy UV field inside the H II region, while the amorphous carbon grains containing more than ~400 C atoms can. The intermediate-sized species probably extend somewhat into the H II region.

5. The 10 μm emission extends farther to the south than the 20 μm thermal radiation, indicating that the UIR features are not thermally excited, but require a nonthermal process such as fluorescence.

6. Wavelength shifts of the 6.2 and 11.3 μm band with position observed when chopping onto the H II region are consistent with anharmonicity effects in PAH molecules.

We wish to thank the many staffs at the observatories that contributed to this research, which included the Kuiper Airborne Observatory, the NASA IRTF, the UKIRT, and the Mount Lemmon 1.5 m telescopes. Without their dedication to providing quality support, these observations would not have been possible. We also have special thanks to Harold Crean for his continuing help in preparing the NASA-Ames equipment for observing.

REFERENCES

Aitken, D. K., Roche, P. F., Spenser, P. M., and Jones, B. 1979, *Astr. Ap.*, **76**, 60.
Allamandola, L. J., Tielens, A. G. G. M., and Barker, J. R. 1985, *Ap. J. (Letters)*, **290**, L25.
———. 1987, in *Polycyclic Aromatic Hydrocarbons and Astrophysics*, ed. A. Leger, L. B. d'Hendecourt, and N. Boccara (Boston: Reidel), p. 255.
Aller, L. H., and Minkowski, R. 1956, *Ap. J.*, **124**, 110.
Barker, J. R., Allamandola, L. J., and Tielens, A. G. G. M. 1987, *Ap. J. (Letters)*, **315**, L61.
Becklin, E. E., Beckwith, S., Gatley, I., Matthews, K., Neugebauer, G., Sarazin, C., and Werner, M. W. 1976, *Ap. J.*, **207**, 770.
Benson, S. W. 1965, *J. Phys. Ed.*, **42**, 502.
Cohen, M., Allamandola, L., Tielens, A. G. G. M., Bregman, J., Simpson, J., Witteborn, F. C., Wooden, D., and Rank, D. 1986, *Ap. J.*, **302**, 737.
Crawford, M. K., Tielens, A. G. G. M., and Allamandola, L. J. 1985, *Ap. J. (Letters)*, **293**, L45.
Dalgarno, A. 1975, in *Atomic and Molecular Processes in Astrophysics*, ed. M. C. E. Huber and H. Nussbaumer (Geneva: Geneva Observatory), p. 11.
deMuizon, M., Geballe, T. R., d'Hendecourt, L. B., and Baas, F. 1986, *Ap. J. (Letters)*, **306**, L105.
Draine, B. T. 1979, *Ap. J.*, **230**, 106.
Duley, W. W., and Williams, D. A. 1981, *M.N.R.A.S.*, **196**, 269.
Dwek, E., Sellgren, K., Soifer, B. T., and Werner, M. W. 1980, *Ap. J.*, **238**, 140.
Geballe, T. R., Allamandola, L. J., Tielens, A. G. G. M., Morehouse, A., and Brand, P. W. J. L. 1989, preprint.
Geballe, T. R., Lacy, G. H., Persson, S. E., MacGregor, P. J., and Soifer, B. T. 1985, *Ap. J.*, **292**, 500.
Goebel, J. H. 1987, in *Polycyclic Aromatic Hydrocarbons and Astrophysics*, ed. A. Leger, L. B. d'Hendecourt, and N. Boccara (Boston: Reidel), p. 329.
Leach, S. 1987, *J. Electron. Spectrosc. Relat. Phenon.*, **41**, 427.
Lèger, A., and d'Hendecourt, L. B. 1987, in *Polycyclic Aromatic Hydrocarbons and Astrophysics*, ed. A. Leger, L. B. d'Hendecourt, and N. Boccara (Boston: Reidel), p. 223.
Lèger, A., and Puget, J. L. 1984, *Astr. Ap. Letters*, **137**, L5.
Martin, A. H. M., and Gull, S. F. 1976, *M.N.R.A.S.*, **175**, 235.
Münch, J., and Taylor, K. 1974, *Ap. J. (Letters)*, **192**, L93.
Robertson, J., and O'Reilly, E. P. 1987, *Phys. Rev. B*, **35**, 2946.
Russell, R. W., Soifer, B. T., and Willner, S. P. 1977, *Ap. J. (Letters)*, **217**, L149.
Sakata, A., Wada, S., Tanabé, T., and Onaka, T. 1984, *Ap. J. (Letters)*, **287**, L51.
Savage, B. D., and Mathis, J. S. 1979, *Ann. Rev. Astr. Ap.*, **17**, 73.
Sellgren, K. 1981, *Ap. J.*, **245**, 138.
———. 1984, *Ap. J.*, **277**, 623.
Tielens, A. G. G. M., Allamandola, L. J., Barker, J. R., and Cohen, M. 1987, in *Polycyclic Aromatic Hydrocarbons and Astrophysics*, ed. A. Leger, L. B. d'Hendecourt, and N. Boccara (Boston: Reidel), p. 273.
Zuckerman, B. 1973, *Ap. J.*, **183**, 863.

L. J. ALLAMANDOLA, J. D. BREGMAN, A. G. G. M. TIELENS, and F. C. WITTEBORN: MS245-6 NASA-Ames Research Center, Moffett Field, CA 94035

T. R. GEBALLE: Joint Astronomy Center, 665 Komohana Street, Hilo, HI 96720